Published in final edited form as:
Nucl Med Biol. 2014 ; 41(10): 785–792. doi:10.1016/j.nucmedbio.2014.08.004.

Inflammation imaging of atherosclerosis in Apo-E-deficient mice using a ^{99m}Tc-labeled dual-domain cytokine ligand

Zhonglin Liu[1,*], **Lilach O. Lerman**[2], **Hui Tang**[2], **Christy Barber**[1], **Li Wan**[1], **Mizhou M. Hui**[3], **Lars R. Furenlid**[1], and **James M. Woolfenden**[1]

[1]Department of Medical Imaging, University of Arizona, Tucson, AZ

[2]Division of Nephrology and Hypertension, Mayo Clinic, Rochester, MN

[3]AmProtein Cooperation, San Gabriel, CA

Abstract

Interleukin-1β (IL-1β) and tumor necrosis factor-α (TNF-α) play a critical role in initiating and accelerating atherosclerosis. This study evaluated the imaging properties of ^{99m}Tc-TNFR2-Fc-IL-1RA (^{99m}Tc-TFI), a dual-domain cytokine radioligand that targets TNF-α and IL-1β pathways, in assessing atherosclerosis development in apolipoprotein-E-deficient (ApoE$^{-/-}$) mice.

Methods—The feasibility and specificity of detecting atherosclerosis with ^{99m}Tc-TFI SPECT imaging were investigated in ApoE$^{-/-}$ and ApoE$^{+/+}$ mice. Fifty-four ApoE$^{-/-}$ mice were fed either an atherogenic diet (AGD) or a normal diet (ND) beginning at 5 weeks of age. Eighteen Apo-E wild-type (ApoE$^{+/+}$) mice were fed a ND. Two groups of ApoE$^{-/-}$ mice (n=12 each group) on AGD and ND were imaged three times with ^{99m}Tc-TFI and a high-resolution SPECT system at 20–25, 30–40, and 48–52 weeks to study the evolution of atherosclerotic plaque.

Results—Focal radioactive accumulations in the aortic arch region were observed in the ApoE$^{-/-}$ mice (n=12) on AGD but not in the ApoE$^{+/+}$ mice on ND (n=10). Apo-E$^{-/-}$ mice on ND (n=11) exhibited lower radioactive uptake than ApoE$^{-/-}$ mice on AGD (P<0.05). Co-injection of an excess of cold ligand with ^{99m}Tc-TFI resulted in significant reduction of ^{99m}Tc-TFI uptake in the ApoE$^{-/-}$ mice on AGD. Longitudinal studies showed that ^{99m}Tc-TFI uptake in the aortas of ApoE$^{-/-}$ mice progressively increased from 20 to 48 weeks. Real-time PCR assays demonstrated that atherosclerotic aortas expressed significantly higher IL-1β and TNF-α than the aortas from wild-type controls.

Conclusions—Atherosclerotic plaques were detected by ^{99m}Tc-TFI imaging in ApoE$^{-/-}$ mice. ^{99m}Tc-TFI is promising for specific detection of inflammatory response in atherosclerotic plaques.

[*]For correspondence or reprints contact: P.O. Box 245067, Tucson, AZ 85724-5067, Phone: 520-626-4248; Fax: 520-626-2892, zliu@radiology.arizona.edu.

Keywords

Atherosclerosis; Interleukin-1; Tumor necrosis factor; Inflammation; SPECT; Apolipoprotein-E-deficient mice

1. Introduction

Atherosclerosis is a chronic inflammatory vascular disease that is mediated by a complex network of pro-inflammatory cytokines, including members of the interleukin family, tumor necrosis factor (TNF), and interferons (IFN) [1]. Molecular imaging of atherosclerotic plaque inflammation may provide an opportunity to measure the inflammatory molecular or cellular components in the plaques and characterize plaque progression and vulnerability [2]. However, imaging of plaque inflammatory components is challenging. The plaques are small, requiring high-spatial-resolution imaging devices for localization. The signal strength of reporter molecules may be weak, necessitating sensitive quantitative techniques for detection. An imaging agent must be able to bind specifically to inflammatory components with high affinity and adequate residence time for imaging. The imaging agent should be rapidly cleared from the circulation to provide sufficient contrast between inflammatory lesions and normal surrounding blood pool and tissues.

In view of the biological importance of Interleukin-1β (IL-1 β) and TNF-α in the development of atherosclerosis [3, 4], imaging of IL-1β and TNF-α activities may be a sensitive indicator of plaque inflammatory reactions and response to therapeutic interventions. IL-1β and TNF-α have coordinated effects in mediating inflammatory reactions [5–7]. A dual-domain fusion protein, TNFR2-Fc-IL-1RA (TFI), has been developed in recent years for functional targeting of IL-1β and TNF-α pathways [8]. TFI consists of a TNF-neutralizing domain that specifically binds to TNF-α, and an IL-1 receptor antagonist domain. We have previously demonstrated that ^{99m}Tc-labeled TFI (^{99m}Tc-TFI) can target inflammatory sites with more potent affinity and increased radioactive uptake compared to the individual cytokine radioligands, ^{99m}Tc-TNFR2-Fc and ^{99m}Tc-IL-1RA-Fc [9, 10]. We hypothesized in this study that ^{99m}Tc-TFI imaging might permit specific assessment of inflammatory reactions in atherosclerotic plaques. To test our hypothesis and determine potential clinical usefulness of ^{99m}Tc-TFI, we performed SPECT imaging studies with ^{99m}Tc-TFI in apolipoprotein-E-deficient (ApoE$^{-/-}$) mice using multiple experimental protocols. We investigated whether interrogation of the inflammatory response via IL-1β and TNF-α pathways could provide monitoring of atherosclerotic plaque evolution.

2. Material and Methods

2.1 Radiolabeling and Cell Binding

TFI was obtained from AmProtein Corporation (San Gabriel, CA). The molecular size of TFI as determined by SDS-PAGE is 84 kDa under reducing conditions and 168 kDa under non-reducing conditions [8]. TFI was ^{99m}Tc-labeled using a modified indirect labeling protocol with succinimidyl 6-hydrazinonicotinate acetone hydrazone (S-HyNic) (Solulink, San Diego, CA) as a chelator [11]. The protein was chelated with S-HyNic at a molar ratio

1:6. HyNic-conjugated TFI (0.1 mg) was mixed with 925 MBq $^{99m}TcO_4^-$ (0.5 ml) in normal saline, 5 μL $SnCl_2$ solution (1 mg/mL), and 200 μL tricine solution (36 mg/mL). The reaction was incubated at room temperature (RT) for 20 minutes to produce ^{99m}Tc-TFI in PBS buffer (pH 7.4). Radiochemical purity (RCP) was determined by size-exclusion high-performance liquid chromatography.

^{99m}Tc-TFI cell binding affinity was determined using isolated polymorphonuclear leukocytes, which were collected from healthy male Sprague-Dawley rats using the hydroxyethyl-starch exchange transfusion method described previously [12]. A total of 5 x 10^5 cells suspended in 1 mL of binding solution were incubated with 2 nM ^{99m}Tc-TFI at varying concentrations of cold TFI for 2 hours at RT. The ligand concentration that inhibited 50% of the maximum specific binding (IC_{50}) to the cells was calculated using the averages of triplicate determinations.

2.2. ApoE$^{-/-}$ Mouse Model

Breeding pairs of ApoE$^{-/-}$ mice were purchased from Jackson Laboratory (Bar Harbor, ME) and bred while consuming a regular diet in the University of Arizona Animal Care Center. Fifty-four offspring ApoE$^{-/-}$ mice were assigned to receive either an atherogenic diet (AGD) containing 1.25% cholesterol, 0% cholate, and 15% fat starting at 5 weeks of age (n=42) or a normal mouse chow (normal diet, ND) containing 4% fat (n=12). ApoE wild-type (ApoE$^{+/+}$) C57BL/6 mice with the same genetic background received ND and served as controls (n=18).

2.3. Experimental Protocols

2.3.1. Feasibility of detecting atherosclerosis in vivo—ApoE$^{-/-}$ mice on AGD (n=12), ApoE$^{-/-}$ mice on ND (n=11), and ApoE$^{+/+}$ mice on ND (n=10), all at 48–52 weeks of age, were used to investigate the feasibility of detecting atherosclerotic plaques with ^{99m}Tc-TFI. These mice had not received any agents earlier in life before ^{99m}Tc-TFI was administered for imaging. The mice received intravenous injections of 111.0–129.5 MBq ^{99m}Tc-TFI in 0.22 mL and underwent SPECT imaging 2–3 times within 24 hours after injection.

2.3.2. ^{99m}Tc-TFI uptake specificity—*In vivo* competitive studies were performed in five ApoE$^{-/-}$ mice on AGD at 48–52 weeks of age. ^{99m}Tc-TFI was co-injected with a 100-fold excess of unlabeled/cold TFI. Aortic radioactivity determined by SPECT imaging and *ex vivo* measurements were compared with and without cold TFI blockade. Saturability in the presence of an excess of cold TFI was studied *in vitro* using fresh aortic slices from two ApoE$^{-/-}$ mice on AGD at 50 weeks of age. Serial pairs of adjacent transverse cryostat slices at 25-μm thickness through the aortic root and arch were collected on glass slides. After pre-incubation in PBS for 5 min, one aortic slice was incubated for 30 min at RT with ^{99m}Tc-TFI at 30 nM concentration in the presence of unlabeled ligand; the adjacent slice was incubated in the absence of competing ligand. The aortic slices were washed twice with PBS and exposed to a phosphor plate and analyzed using a Fujifilm BAS-5000 system (Fujifilm Medical Systems USA, Stamford, CT). The aortic slices were counted using a gamma well

counter. The difference between averaged slice counts with and without blockade was analyzed statistically.

2.3.3. Longitudinal studies—Twenty-four ApoE$^{-/-}$ mice were divided into groups on AGD (n=12) and ND (n=12) to study the evolution of atherosclerotic plaque. Five ApoE$^{-/-}$ mice on AGD and six on ND were imaged three times at 20–25, 30–40, and 48–52 weeks. At each session SPECT images were acquired at 0.5–1, 3 and 24 hours after 111.0–129.5 MBq ^{99m}Tc-TFI injection (0.22 mL). The other seven ApoE$^{-/-}$ mice on AGD and six mice on ND were euthanized with either no images or after imaging only 1–2 times within 20–40 weeks of age because of progressive skin lesions likely due to high plasma cholesterol level. After each imaging study, the animals were recovered and housed until the final study.

2.4. SPECT Image Acquisition and Analysis

All mice were anesthetized with 1.0–1.5% isoflurane. ^{99m}Tc-TFI was injected through the tail vein. Each mouse was imaged multiple times up to 24 hours using a stationary SPECT imager, FastSPECT II. Its spatial resolution is about 1 mm with a 16-pinhole aperture. The mouse was positioned with the field of view covering the entire chest and neck area. Projection data were acquired for 5–20 minutes based on the injected dose and time after injection.

Reconstructions of FastSPECT II data were processed using 50 iterations of the OS-EM algorithm. Using AMIDE 0.9.2 software, tomographic transverse, coronal, and sagittal slices with one-voxel thickness (0.5 mm) were produced. An image was interpreted as positive if focal uptake (hot spot) was localized to the region of the aorta on at least three adjacent tomographic slices. Visual sub-classification was performed on focal activity 3 hours post-injection as follows: 0 = equal to soft-tissue radioactive background, 1 = slightly higher accumulation than soft-tissue background, 2 = focal uptake and activity lower than liver, 3 = focal uptake and activity equal to liver, and 4 = focal uptake and activity higher than liver. In addition, using the line profile function of Amide software, relative pixel intensities were determined over the lesions in the aortic areas for semi-quantitative assessment of radioactive uptake.

2.5. Postmortem Analysis

At the end of the final imaging session, mice were euthanized. The entire aorta, brachiocephalic trunk and carotid arteries were harvested and weighed. Radioactivity (%ID/g) in the whole aorta was determined by gamma-well counting.

Atherosclerotic plaques were evaluated by Oil Red O staining of intact aortas in 6 ApoE$^{-/-}$ mice on AGD, 6 ApoE$^{-/-}$ mice on ND, and 5 ApoE$^{+/+}$ mice on ND at 48–52 weeks of age. The aortic specimens were rinsed with 60% 2-propanol for 3 min and incubated in Oil Red O solution at 37°C for 40 min. Stained samples were mounted on glass slides for autoradiography. In another procedure, the entire aorta was harvested as described above in 6 ApoE$^{-/-}$ mice on AGD, 5 ApoE$^{-/-}$ mice on ND, and 5 ApoE$^{+/+}$ mice on ND at 48–52 weeks of age. The segment of ascending aorta and aortic arch was cut off and fixed with 10% paraformaldehyde for histological examination. The thoracic and abdominal segments

were longitudinally incised, mounted on glass slides, stained with Oil Red O, photographed, and evaluated by autoradiography. The autoradiograph exposure time of the samples varied from 20 minutes to 3 hours depending on the aortic radioactivity. Photographs and autoradiographs were evaluated side by side based on anatomical landmarks to clarify the presence of plaque and radioactive uptake. A numerical index was determined based on lesion size and intensity of Oil Red O staining: 0 = no lesions, not stained; 1 = small lesions, slightly stained; 2 = scattered lesions, moderately stained; 3 = lesions covering up to 50% of the aortic wall, intensely stained; 4 = lesions covering more than 50% of the aortic wall, very intensely stained.

Fixed ascending-aorta and aortic-arch specimens were embedded in paraffin and cut at 5-μm thickness. Histological sections were stained with hematoxylin-eosin (H&E) to evaluate the overall architecture, presence of atherosclerotic plaque, and inflammatory cell infiltration. The expression of IL-1β and TNF-α in the plaques was evaluated after immunostaining the paraffin sections with rabbit monoclonal antibody (mAb). All procedures, including staining of the tissue sections, deparaffinization, and cell conditioning (antigen retrieval with a borate-EDTA buffer) were performed on a Discovery XT Automated Immunostainer (Ventana Medical Systems, Inc., Tucson, AZ), using Ventana-validated reagents. Rabbit IL-1β and TNF-α mAb were detected using an anti-rabbit biotinylated secondary mAb followed by biotinylated streptavidin-horseradish peroxidase and 3,3′-diaminobenzidine. Primary antibody staining was detected by hematoxylin counterstaining. Following staining, slides were dehydrated through graded alcohols, cleared in xylene, and cover-slipped with mounting medium. Images were captured using a Nikon microscope with digital image software.

2.6. Measurement of IL-1β and TNF-α by real-time PCR

Quantitative real-time PCR (qRT-PCR) data were obtained in ApoE$^{-/-}$ mice on AGD (n=6, 20 weeks old; n=4, 30–52 weeks old) and ND (n=4, 20 weeks old; n=4, 30–52 weeks old). The ApoE$^{-/-}$ mice had previously received one or more injections of ^{99m}Tc-TFI. Eight ApoE$^{+/+}$ mice on ND (n=4, 20 weeks old: n=5, 30–52 weeks old), which had not been used in any other studies, served as controls. The whole aorta from ascending segment to abdominal aorta was harvested and kept at −80°C until the time of qRT-PCR. Total RNA was isolated using a mirVana™ PARIS™ total RNA isolation kit (Life Technologies, Grand Island, NY). First-strand cDNA was produced from 50 ng of total RNA using a SuperScript VILO cDNA Synthesis kit, and qRT-PCR was performed in triplicate on cDNA using the Taqman gene expression assay. The primer pairs from Life Technologies were TNF-α: Mm00443260_g1, and IL-1β: Mm00434228_m1. GAPDH was used as an internal control. Negative controls with no cDNA were cycled in parallel with each run. Fold changes of each target gene in the experiment groups relative to the control group were calculated using the $2^{-\Delta\Delta CT}$ method, where CT (threshold cycles) is the number of cycles that the fluorescence generated crosses a threshold and ΔCT is relative fold change in gene expression (ΔCT = CT/target gene − CT/GAPDH). PCR data were analyzed based on ΔCT values (ΔΔCT) in ApoE$^{-/-}$ mice compared to those in wild-type controls.

2.7. Data Analysis

All quantitative results were expressed as mean ± S.E.M. Comparisons between two variables were performed with one-way analysis of variance. Probability values less than 0.05 were considered significant.

2.8. Ethics

The animal experiments were carried out in compliance with the Principles of Laboratory Animal Care from the National Institutes of Health (NIH Publication 85-23, revised 1985) and were approved by the Institutional Animal Care and Use Committee (IACUC) at the University of Arizona.

3. Results

3.1. Radiolabeling and Cell Binding

The radiolabeling yield of ^{99m}Tc-TFI was typically greater than 80%. After gel purification, ^{99m}Tc-TFI RCP was always greater than 98% for animal injection. Binding of ^{99m}Tc-TFI to leukocytes gradually decreased with addition of increasing amounts of non-radiolabeled TFI, as shown in Fig. 1. The IC_{50} for ^{99m}Tc-TFI was 48.04 nM (n=3).

3.2. Feasibility of detecting atherosclerosis in vivo

In 48–52-week-old ApoE$^{-/-}$ mice on AGD, focal radioactive accumulation (hot spot) in the aortic arch region became visible around 60 minutes and remained detectable over the 3–24 hour post-injection period. Representative ^{99m}Tc-TFI images of an ApoE$^{-/-}$ mouse on AGD at age 50 weeks are shown in Fig. 2(A–F). Radioactive uptake in the aortic lesions of ApoE$^{-/-}$ mice on AGD was 14-fold (14.2±1.3) higher than radioactive distribution in chest wall, based on line-profile analysis. ApoE$^{-/-}$ mice on ND exhibited less aortic uptake than ApoE$^{-/-}$ mice on AGD, with uptake only 6.8±1.1 times higher than soft-tissue background (P<0.05 vs. AGD). ^{99m}Tc-TFI accumulation was barely detectable in ApoE$^{+/+}$ mice on ND, as shown in Fig. 2(G–L); profile analysis showed that aortic uptake was 1.52±0.43 times higher than the chest wall background and significantly lower than that in ApoE$^{-/-}$ mice on AGD or ND (P<0.01 for both comparisons).

3.3. Specificity of ^{99m}Tc-TFI Uptake

In vivo blockade by unlabeled TFI induced a significant decrease in radioactive uptake of ^{99m}Tc-TFI in aortic plaque in ApoE$^{-/-}$ mice. The radioactivity (%ID/g) with blockade was reduced to 0.36±0.05 compared to 1.27±0.15 in those without blockade (P<0.01). The specificity of ^{99m}Tc-TFI uptake in plaque was further evident by *in vitro* tissue binding studies on slices of aortic arch samples incubated with and without blockade (Fig. 3). The bound radioactivity (% of total ^{99m}Tc activity) was significantly reduced in the slices with cold ligand blocking compared to that without blocking (6.2±1.1 vs. 49.7±8.6, P<0.001).

3.4. Longitudinal Imaging Results

ApoE$^{-/-}$ mice on ND exhibited slower development of plaques and lower radioactive uptake in the aorta than ApoE$^{-/-}$ mice on AGD, as shown in Fig. 4 (row A–C). Radioactive lesions

were typically detectable starting at age 30 weeks. The aortic lesions became prominent at 48–52 weeks. Focal aortic uptake of ^{99m}Tc-TFI in the ApoE$^{-/-}$ mice on AGD increased from 20–25 weeks to 48–52 weeks (Fig. 4, row D–F), suggesting growth of plaque. At age 20–25 weeks, focal uptake in the aortic region was readily detectable. Around 30–40 weeks, the radioactive lesions became more significant and the carotid arteries also demonstrated focal radioactive accumulation. By 48–52 weeks, radioactive lesions were prominent in the aortic arch and carotid arteries. Representative profile changes of aortic radioactive uptake in the longitudinal study are shown in Fig. 4(G and H).

3.5. Postmortem Analysis

Ex vivo levels (%ID/g) of ^{99m}Tc-TFI were significantly higher in the aortas of ApoE$^{-/-}$ mice on AGD (1.27±0.15) than in ApoE$^{-/-}$ mice on ND (0.73±0.14) (P<0.01). ^{99m}Tc-TFI aortic uptake in both of these groups was significantly higher than that in ApoE$^{+/+}$ control mice on ND (0.33±0.02) (P<0.01 for both comparisons).

Oil Red O staining and autoradiography demonstrated prominent atherosclerotic lesions with high radioactive uptake in the aortic arch, brachiocephalic trunk, and carotid arteries of ApoE$^{-/-}$ mice on AGD, as shown in Fig. 5(A–F). In ApoE$^{-/-}$ mice on ND, stained atherosclerotic lesions were also observed in aortas, especially aortic arches, but lesion size, number, and radioactivity were markedly less than in the ApoE$^{-/-}$ mice on AGD. There were few stained lesions in aortas from ApoE$^{+/+}$ control mice on ND, and ^{99m}Tc-TFI accumulation was barely detectable by autoradiography. In the longitudinally incised thoracic-abdominal aorta from ApoE$^{-/-}$ mice on AGD, multiple plaques were clearly observed on the luminal surface, as shown in Fig. 5(G–L). Autoradiography showed good consistency between ^{99m}Tc-TFI accumulation and Oil Red O staining. ApoE$^{-/-}$ mice on ND also exhibited plaques and increased ^{99m}Tc-TFI accumulation, but there were fewer plaques with less staining and lower radioactive uptake. ApoE$^{+/+}$ controls showed tiny lipid depositions on the luminal surface, with barely noticeable radioactive accumulations. Estimated indexes of atherosclerotic lesions by Oil Red O and FastSPECT II imaging were similar, as shown in Fig. 6. Respective values were 0.83±0.31 vs. 1.00 ±0.26 (P>0.05) in ApoE$^{+/+}$ mice on ND; 1.83±0.40 vs. 2.33 ± 0.33 (P>0.05) in ApoE$^{-/-}$ mice on ND, and 3.17±0.31 vs. 3.33±0.21 (P>0.05) in ApoE$^{-/-}$ mice on AGD.

H&E staining showed that atherosclerotic plaques were mainly observed in the aortic root, aortic arch, and abdominal aorta in the ApoE$^{-/-}$ mice on AGD. Fewer atherosclerotic lesions were found in thoracic aortic segments. Fig. 7A is a representative microscopic image of atherosclerotic aortic arch from an ApoE$^{-/-}$ mouse on AGD at age 50 weeks, in which plaque with intense inflammatory reaction is present. Similar plaque and inflammatory cell recruitment were found in all examined ApoE$^{-/-}$ mice on AGD at 48–52 weeks of age, but not in the ApoE$^{+/+}$ mice on ND, as shown in Fig. 7D. Histologic sections from areas with lower ^{99m}Tc-TFI uptake showed less inflammatory infiltration, and sections from areas with higher ^{99m}Tc-TFI uptake exhibited stronger inflammatory response. Immunohistochemical examination showed that expression of IL-1β and TNF-α was up-regulated in the atherosclerotic plaques in ApoE$^{-/-}$ mice on AGD (Fig. 7B and 7C), but not in ApoE$^{+/+}$ mice (Fig. 7E and 7F).

3.6. IL-1β and TNF-α qRT-PCR assays

The results of qRT-PCR assays are summarized in Fig. 8. IL-1β RNA levels in ApoE$^{-/-}$ mice on both AGD and ND were significantly higher at 30–52 weeks compared to ApoE$^{+/+}$ mice (P<0.001 for both comparisons). TNF-α levels in ApoE$^{-/-}$ mice on AGD, but not on ND, were higher than those in ApoE$^{+/+}$ mice on ND (P=0.002). Moreover, the levels of IL-1β and TNF-α in ApoE$^{-/-}$ mice on AGD were significantly higher at 30–52 weeks of age than at 20 weeks (P<0.001 and P<0.05, respectively). There was a significant difference in the level of IL-1β RNA between the ApoE$^{-/-}$ mice on AGD and ND (P<0.05). However, the difference in TNF-α between these groups did not reach statistical significance.

4. Discussion

Cytokine-based SPECT imaging could be a specific measure of plaque development linked directly to inflammatory response. Previously, ^{99m}Tc-labeled interleukin-2 (IL-2) uptake in carotid plaques was used to measure absolute number of lymphocytes expressing IL-2 receptors in the plaque, suggesting that non-invasive cytokine imaging can allow quantification of atherosclerotic plaque inflammation [13]. ^{99m}Tc-TFI imaging data in this study provides implications for clinical detection of atherosclerotic inflammation via IL-1 and TNF pathways, as these two pro-inflammatory cytokines play a critical role in atherosclerosis from initiation to destabilization.

IL-1β binds to Type I IL-1 receptors (IL-1RI), which are expressed on the cell membrane of vascular endothelial cells, smooth muscle cells, and inflammatory cells. Upregulation of IL-1β results in high IL-1RI expression in atherosclerotic vessels [14]. IL-1β binding promotes release of metalloproteinase that breaks down the connective tissue matrix of the plaque and makes the plaque vulnerable [15, 16]. The carboxy-terminal IL-1RA sequence of ^{99m}Tc-TFI acts as a competitive receptor antagonist for binding of IL-1, and it has higher binding affinity for IL-1RI than do IL-1α and IL-1β [17]. ^{99m}Tc-TFI uptake therefore reflects the expression of IL-1β in atherosclerotic aortas by IL-1RI binding.

TNF-α is believed to participate in every step of inflammation from atherosclerotic initiation to destabilization [18–20]. When the carboxy-terminal sequence of ^{99m}Tc-TFI binds to IL-1RI, the amino-terminal segment (TNFR2) domain retains the ability to bind to its targets on TNF-producing cells, including membrane-bound TNF (mTNF) and soluble TNF (sTNF) [21, 22]. TNFR2 binds with higher affinity to mTNF than to sTNF [23–25]. It is possible that ^{99m}Tc-TFI bound predominately to mTNF in the inflammatory plaques of our ApoE$^{-/-}$ mouse models. When the TNFR2 domain binds to mTNF/sTNF, the IL-1RA domain may bind to IL-1RI on other cell membranes.

The atherosclerotic plaques in ApoE$^{-/-}$ mice exhibit upregulated cytokines and provide a platform to evaluate the targeting properties of ^{99m}Tc-TFI. Feeding the ApoE$^{-/-}$ mice an AGD accelerated the atherosclerotic plaque formation and resulted in enhanced ^{99m}Tc-TFI uptake. The ApoE$^{-/-}$ mouse model resembles human atherosclerosis in that the most prominent cells involved in lesion development are monocyte-derived macrophages and T-lymphocytes [4, 26]. The ^{99m}Tc-TFI imaging data in the ApoE$^{-/-}$ model support the feasibility of clinical detection of atherosclerotic inflammation via IL-1 and TNF pathways.

The experimental results in this study suggest that increased uptake of ^{99m}Tc-TFI in the early stage of atherosclerotic plaques may be primarily due to the IL-1 pathway, whereas in a more advanced stage of plaque development, both IL-1 and TNF pathways may contribute to ^{99m}Tc-TFI uptake. These two pro-inflammatory cytokines play a critical role in atherosclerotic destabilization, but this study was not designed to evaluate progression to rupture of vulnerable plaque. We plan further studies using this dual-domain cytokine radioligand to assess inflammatory responses leading to plaque vulnerability and rupture.

There are limitations to this study. When animal SPECT images were collected in this study, a micro-CT was unavailable for dual-modality imaging in our laboratory. Co-registered CT contrast images would be very helpful to localize focal radioactive uptake in the mouse aorta on SPECT images. Liver and intestinal ^{99m}Tc-TFI activity may hinder detection of plaque in the abdominal aorta. Some uptake of ^{99m}Tc-TFI in the aorta may result from non-specific uptake due to increased endothelial permeability and intra-plaque neovascularization; further studies using a control molecule similar in size to TFI would be useful. Total RNA in this study was extracted from the whole aortas, not exclusively from the plaques, and thus mRNA levels of IL-1β and TNF-α measured by qRT-PCR assays might represent an averaged cytokine profile and not just the cytokine expression in the plaques. This technical drawback may explain why the difference in mRNA levels of IL-1β and TNF-α between the Apo$^{-/-}$ and Apo$^{+/+}$ mice was relatively faint although statistically significant.

5. Conclusion

Atherosclerotic plaques in ApoE$^{-/-}$ mice were noninvasively detected by high-resolution SPECT imaging using ^{99m}Tc-TFI. This dual-domain cytokine radioligand showed increasing uptake during plaque evolution, as confirmed by histological examinations and cytokine measurements. Bifunctional imaging with ^{99m}Tc-TFI may exploit the synergy between IL-1β and TNF-α pathways and may enable characterization of vascular plaques undergoing inflammation at different phases. Further studies are warranted to determine if ^{99m}Tc-TFI SPECT imaging is a feasible and specific tool with which to identify vulnerable plaque in patients at high risk of atherosclerotic complications, thereby promoting timely therapy to prevent plaque rupture and cardiovascular death.

Acknowledgments

The authors wish to thank Dr. Gail Stevenson for support in animal studies. We thank Edward Abril from the University of Arizona Tissue Acquisition and Cellular/Molecular Analysis Shared Service, which is supported by the Arizona Cancer Center Grant (NIH CA023074), for generating the histological data. This work was supported by NIH grants NHLBI R01-HL090716 and NIBIB P41-EB002035. Dr. Mizhou Hui is Chief Scientific Officer of AmProtein Corporation.

References

1. ten Kate GL, Sijbrands EJ, Staub D, Coll B, ten Cate FJ, Feinstein SB, et al. Noninvasive imaging of the vulnerable atherosclerotic plaque. Curr Probl Cardiol. 2010; 35:556–91. [PubMed: 20974314]
2. Kaufmann BA, Carr CL, Belcik JT, Xie A, Yue Q, Chadderdon S, et al. Molecular imaging of the initial inflammatory response in atherosclerosis: implications for early detection of disease. Arterioscler Thromb Vasc Biol. 2010; 30:54–9. [PubMed: 19834105]

3. Hansson GK, Libby P, Schonbeck U, Yan ZQ. Innate and adaptive immunity in the pathogenesis of atherosclerosis. Circ Res. 2002; 91:281–91. [PubMed: 12193460]
4. Kleemann R, Zadelaar S, Kooistra T. Cytokines and atherosclerosis: a comprehensive review of studies in mice. Cardiovasc Res. 2008; 79:360–76. [PubMed: 18487233]
5. Cain BS, Meldrum DR, Dinarello CA, Meng X, Joo KS, Banerjee A, et al. Tumor necrosis factor-alpha and interleukin-1beta synergistically depress human myocardial function. Crit Care Med. 1999; 27:1309–18. [PubMed: 10446825]
6. Kan H, Xie Z, Finkel MS. TNF-alpha enhances cardiac myocyte NO production through MAP kinase-mediated NF-kappaB activation. Am J Physiol. 1999; 277:H1641–6. [PubMed: 10516205]
7. Bendele AM, Chlipala ES, Scherrer J, Frazier J, Sennello G, Rich WJ, et al. Combination benefit of treatment with the cytokine inhibitors interleukin-1 receptor antagonist and PEGylated soluble tumor necrosis factor receptor type I in animal models of rheumatoid arthritis. Arthritis and rheumatism. 2000; 43:2648–59. [PubMed: 11145022]
8. Xie B, Liu S, Wu S, Chang A, Jin W, Guo Z, et al. A novel bifunctional protein TNFR2-Fc-IL-1ra (TFI): expression, purification and its neutralization activity of inflammatory factors. Mol Biotechnol. 2013; 54:141–7. [PubMed: 22565853]
9. Liu Z, Wyffels L, Barber C, Wan L, Xu H, Hui MM, et al. Characterization of 99mTc-labeled cytokine ligands for inflammation imaging via TNF and IL-1 pathways. Nucl Med Biol. 2012; 39:905–15. [PubMed: 22749187]
10. Liu Z, Barber C, Wan L, Liu S, Hui MM, Furenlid LR, et al. SPECT imaging of inflammatory response in ischemic-reperfused rat hearts using a 99mTc-labeled dual-domain cytokine ligand. J Nucl Med. 2013; 54:2139–45. [PubMed: 24179185]
11. Blankenberg FG, Vanderheyden JL, Strauss HW, Tait JF. Radiolabeling of HYNIC-annexin V with technetium-99m for in vivo imaging of apoptosis. Nat Protoc. 2006; 1:108–10. [PubMed: 17406220]
12. Liu Z, wyffels L, Barber C, Hui MM, Woolfenden JM. A (99m)Tc-labeled dual-domain cytokine ligand for imaging of inflammation. Nucl Med Biol. 2011; 38:795–805. [PubMed: 21843776]
13. Annovazzi A, Bonanno E, Arca M, D'Alessandria C, Marcoccia A, Spagnoli LG, et al. 99mTc-interleukin-2 scintigraphy for the in vivo imaging of vulnerable atherosclerotic plaques. Eur J Nucl Med Mol Imaging. 2006; 33:117–26. [PubMed: 16220305]
14. Olofsson PS, Sheikine Y, Jatta K, Ghaderi M, Samnegard A, Eriksson P, et al. A functional interleukin-1 receptor antagonist polymorphism influences atherosclerosis development. The interleukin-1beta:interleukin-1 receptor antagonist balance in atherosclerosis. Circ J. 2009; 73:1531–6. [PubMed: 19574724]
15. Merhi-Soussi F, Kwak BR, Magne D, Chadjichristos C, Berti M, Pelli G, et al. Interleukin-1 plays a major role in vascular inflammation and atherosclerosis in male apolipoprotein E-knockout mice. Cardiovasc Res. 2005; 66:583–93. [PubMed: 15914123]
16. Shemesh S, Kamari Y, Shaish A, Olteanu S, Kandel-Kfir M, Almog T, et al. Interleukin-1 receptor type-1 in non-hematopoietic cells is the target for the pro-atherogenic effects of interleukin-1 in apoE-deficient mice. Atherosclerosis. 2012; 222:329–36. [PubMed: 22236482]
17. Efthimiou P, Markenson JA. Role of biological agents in immune-mediated inflammatory diseases. South Med J. 2005; 98:192–204. [PubMed: 15759950]
18. Vilcek J, Lee TH. Tumor necrosis factor. New insights into the molecular mechanisms of its multiple actions. J Biol Chem. 1991; 266:7313–6. [PubMed: 1850405]
19. Popa C, Netea MG, van Riel PL, van der Meer JW, Stalenhoef AF. The role of TNF-alpha in chronic inflammatory conditions, intermediary metabolism, and cardiovascular risk. J Lipid Res. 2007; 48:751–62. [PubMed: 17202130]
20. Lamon BD, Hajjar DP. Inflammation at the molecular interface of atherogenesis: an anthropological journey. Am J Pathol. 2008; 173:1253–64. [PubMed: 18948435]
21. Van Zee KJ, Kohno T, Fischer E, Rock CS, Moldawer LL, Lowry SF. Tumor necrosis factor soluble receptors circulate during experimental and clinical inflammation and can protect against excessive tumor necrosis factor alpha in vitro and in vivo. Proc Natl Acad Sci U S A. 1992; 89:4845–9. [PubMed: 1317575]

22. Fernandez-Botran R, Crespo FA, Sun X. Soluble cytokine receptors in biological therapy. Expert Opin Biol Ther. 2002; 2:585–605. [PubMed: 12171504]

23. Bradley JR. TNF-mediated inflammatory disease. J Pathol. 2008; 214:149–60. [PubMed: 18161752]

24. MacEwan DJ. TNF receptor subtype signalling: differences and cellular consequences. Cell Signal. 2002; 14:477–92. [PubMed: 11897488]

25. Tracey D, Klareskog L, Sasso EH, Salfeld JG, Tak PP. Tumor necrosis factor antagonist mechanisms of action: a comprehensive review. Pharmacol Ther. 2008; 117:244–79. [PubMed: 18155297]

26. Daugherty A. Mouse models of atherosclerosis. Am J Med Sci. 2002; 323:3–10. [PubMed: 11814139]

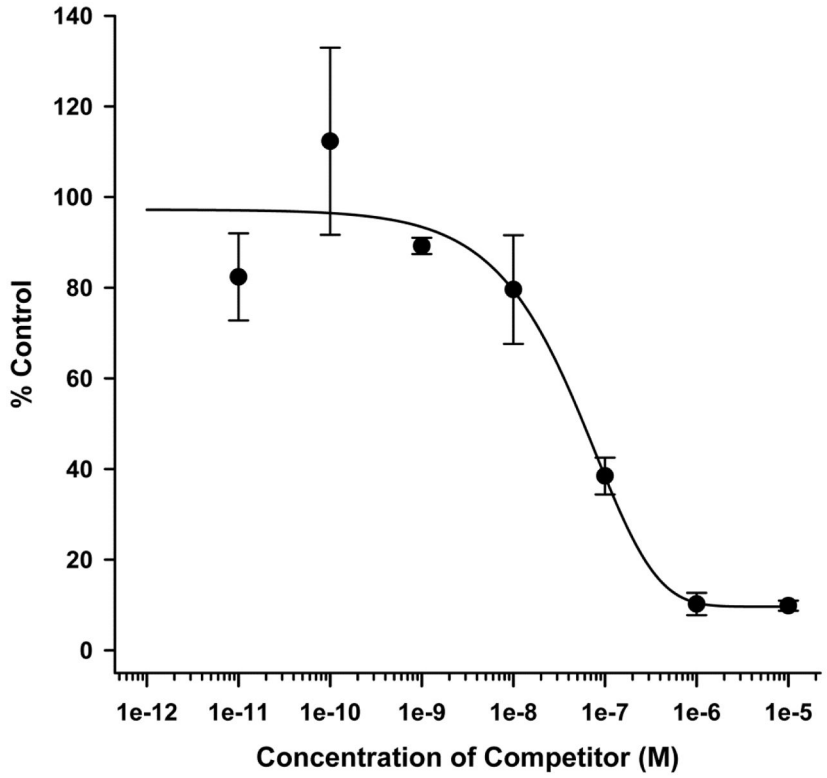

Fig. 1.

Results of *in vitro* competitive cell binding of ^{99m}Tc-TFI and unlabeled TFI (competitor) using isolated rat leukocytes.

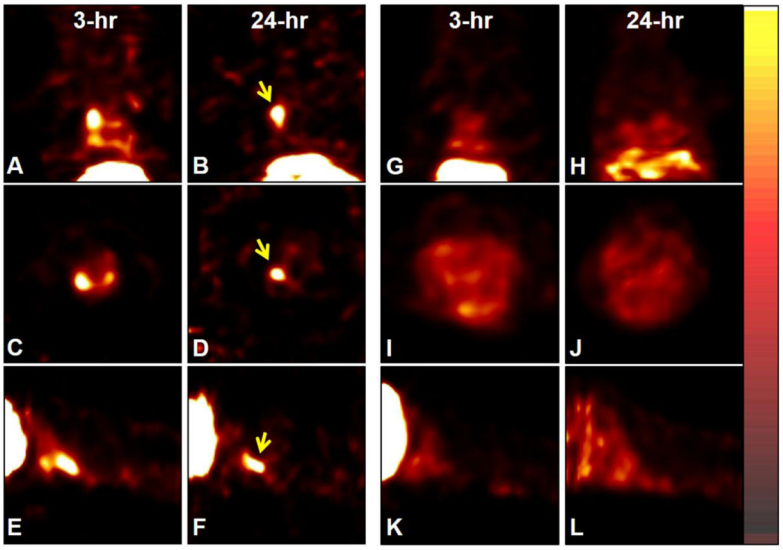

Fig. 2.

Coronal, transverse, and sagittal slices of ^{99m}Tc-TFI SPECT images (0.5 mm/slice) in an ApoE$^{-/-}$ mouse on AGD (**A**–**F**) and ApoE$^{+/+}$ mouse (**G**–**L**) at age 50 weeks. The mice were anesthetized with 1.0% isoflurane and received 114.7 and 122.1 MBq ^{99m}Tc-TFI. The imaging data were acquired for 5 and 15 minutes at 3 and 24 hours post-injection, respectively. Focal radioactive accumulations (arrows) are visualized in the aortic area above the heart in the ApoE$^{-/-}$ mouse at 3 hours (**A**, **C**, **E**) and 24 hours (**B**, **D**, **F**) post-injection, but not in the corresponding site (**G**–**L**) in the ApoE$^{+/+}$ mouse.

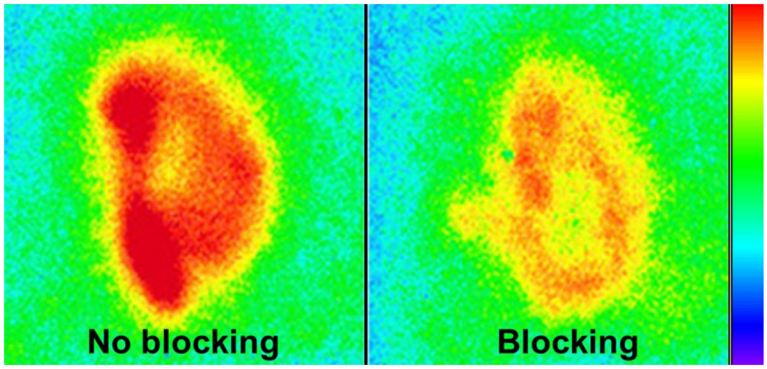

Fig. 3.

Representative ^{99m}Tc-TFI autoradiographs of *a*djacent aortic slices from a 52-week-old ApoE$^{-/-}$ mouse in the absence (no blocking) and presence (blocking) of cold TFI. The slices were simultaneously exposed on the same phosphor plate with the scale set at the same quantitative value. The bound radioactivity was significantly reduced in the slice with blocking compared to that without blocking.

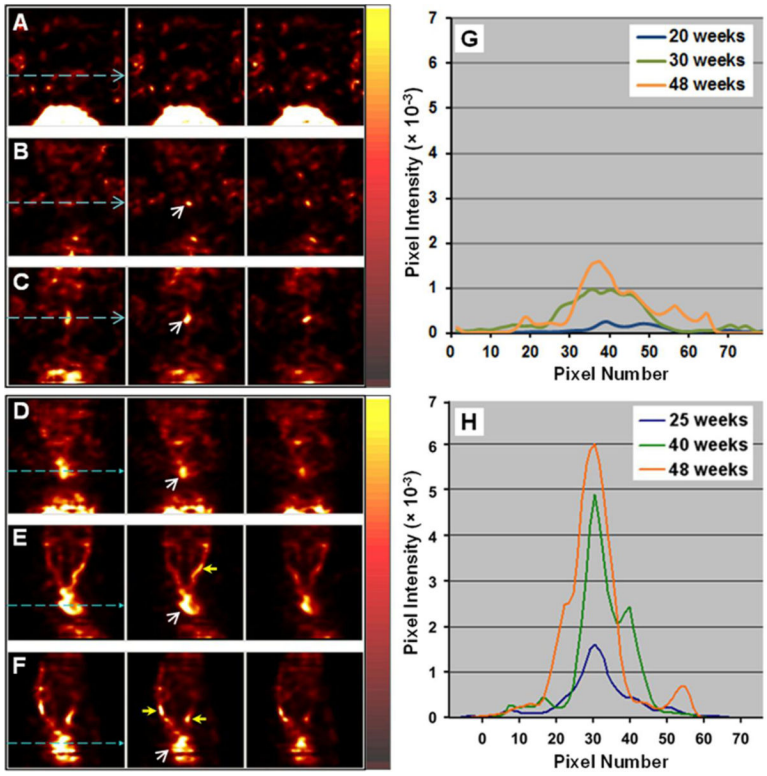

Fig. 4.

^{99m}Tc-TFI SPECT images (three adjacent coronal slices) of one ApoE$^{-/-}$ mouse on ND at age 20 (A), 30 (B), and 48 (C) weeks, and another ApoE$^{-/-}$ mouse on AGD at age 25 (D), 40 (E), and 48 (F) weeks. The mice were anesthetized with 1.0% isoflurane and received intravenous injection of 111.0–129.5 MBq ^{99m}Tc-TFI at each time. The imaging data were acquired for 10 minutes at 3 hours post-injection. Starting at 30 weeks, the aortic area in the ND mouse demonstrated focal radioactive uptake (white arrow), which became more evident at 48 weeks. Higher focal radioactivity (white arrow) was observed in the aortic area of the AGD mouse from 25 to 48 weeks and increased at later times. At 40 and 48 weeks, the carotid arteries (yellow arrows) in the AGD mouse demonstrated focal uptake. Semi-quantitative profile analysis at the levels marked by light-blue dashed lines showed progressive increase in relative pixel intensity indicative of radioactivity over the aortic lesions of representative mice on ND (G) and AGD (H).

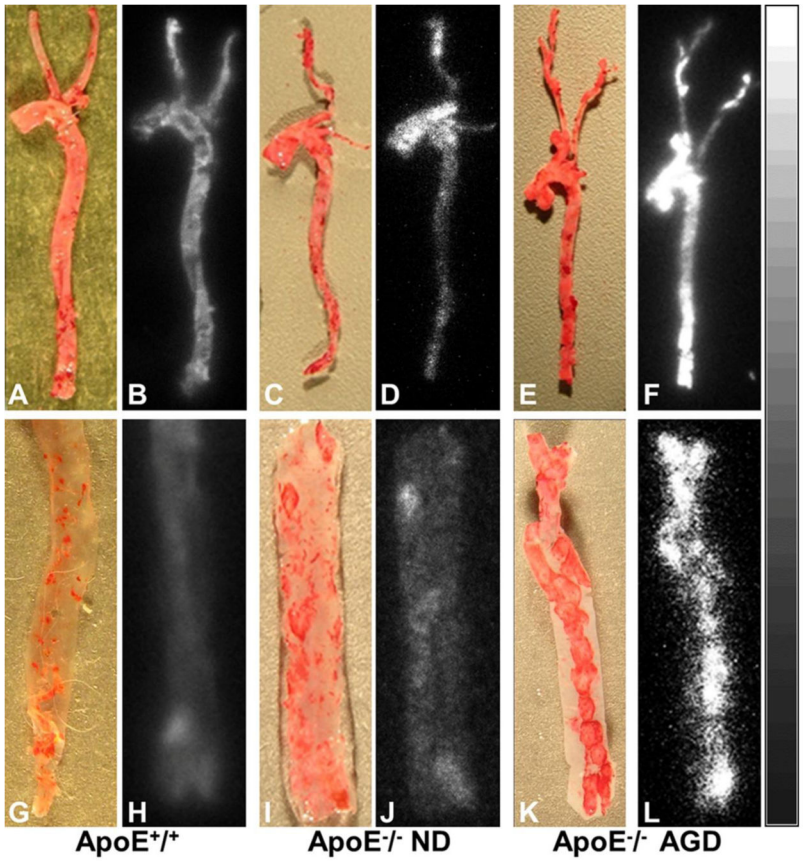

Fig. 5.

Photographs of Oil Red O staining vs. autoradiographs of intact mouse aortas (top row) and incised aortic segments (bottom row) from an ApoE^{+}/$^{+}$ mouse (**A**, **B**, **G,** and **H**), ApoE^{-}/$^{-}$ mouse on ND (**C**, **D**, **I,** and **J)**, and ApoE^{-}/$^{-}$ mouse on AGD (**E**, **F**, **K,** and **L**) at age 48–52 weeks. Autoradiographs showed significantly higher radioactive uptake in aortic and carotid artery lesions stained by Oil Red O in the Apo-E^{-}/$^{-}$ mouse on AGD (**F**, **L**), but barely detectable radioactive accumulations in the corresponding vessels of the ApoE^{+}/$^{+}$ mouse (**B**, **H**). The ApoE^{-}/$^{-}$ mouse on ND exhibited slightly increased uptake in the aorta and carotid artery (**D**, **J**).

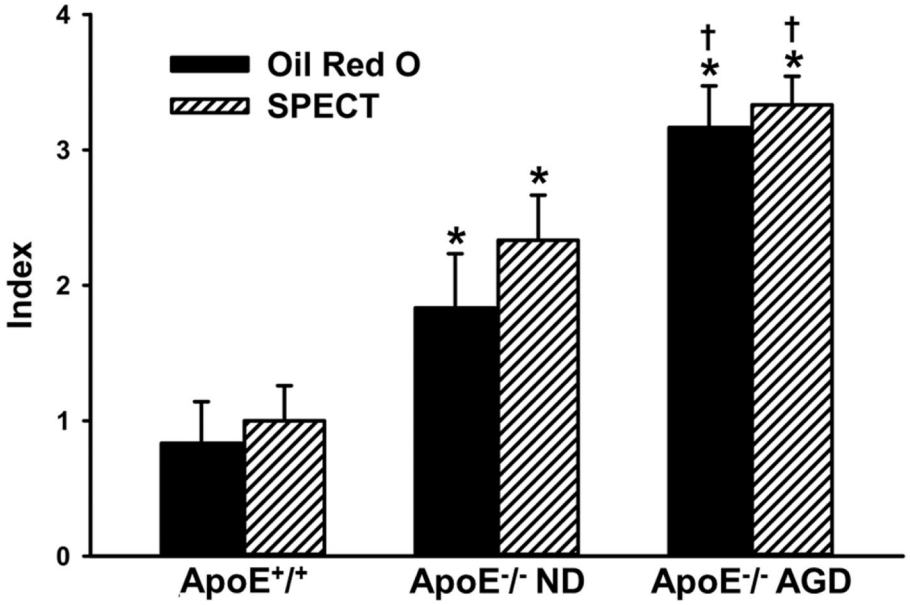

Fig. 6.

Estimated indexes of atherosclerotic aortic lesions by SPECT imaging and post-mortem Oil red O staining. * = $P < 0.05$ compared to $ApoE^{+}/^{+}$. † = $P < 0.05$ compared to $ApoE^{-}/^{-}$ on ND. There was no significant difference between SPECT and Oil red O assessment ($P > 0.05$).

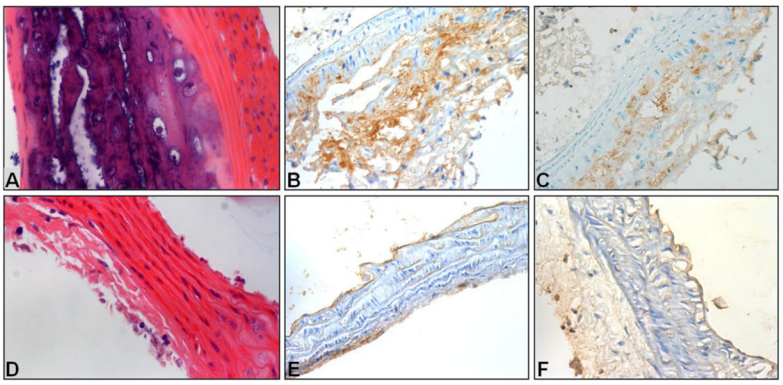

Fig. 7.

Histologic images (magnifications: 40x) of sections from the aortic arch of an ApoE$^{-/-}$ mouse on AGD and ApoE$^{+/+}$ mouse on ND, both at 50 weeks of age. Hematoxylin-eosin staining showed atherosclerotic plaque on the aortic arch of the ApoE$^{-/-}$ mouse (**A**) and no plaque on ApoE$^{+/+}$ mouse (**D**). Immunohistochemical assays with anti-IL-1β and TNF-α antibodies showed strong IL-1β and TNF-α expression in the aortic arch of the ApoE$^{-/-}$ mouse (**B** and **C**), but not in the ApoE$^{+/+}$ mouse (**E** and **F**).

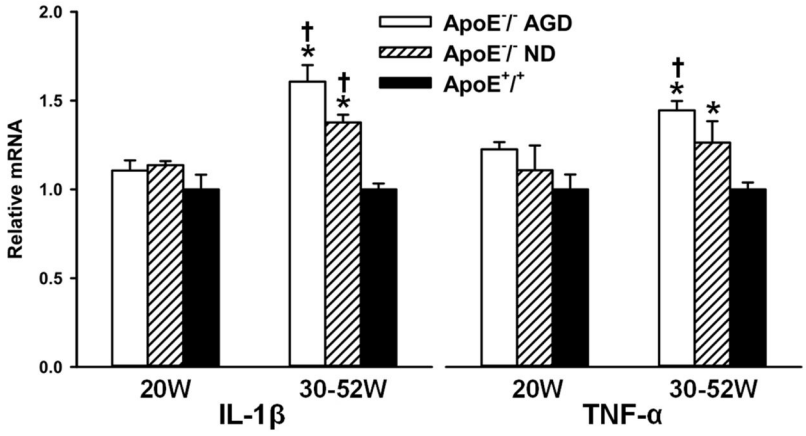

Fig. 8.

Results of qRT-PCR analysis of IL-1β and TNF-α in homogenized aortas of ApoE$^{-/-}$ mice on AGD, ApoE$^{-/-}$ mice on ND, and ApoE$^{+/+}$ mice. Specimens were obtained from animals at ages of 20 weeks and 30–52 weeks. * = P<0.05 compared to ApoE$^{+/+}$ at 30–52 weeks. † = P < 0.05 compared to corresponding ApoE$^{-/-}$ at 20 weeks.